ELSEVIER

SCIENCE DIRECT®

PHYSICS LETTERS B

Physics Letters B 559 (2003) 171–178

www.elsevier.com/locate/npe

Experimental study of the $e^+e^- \to \pi^0\gamma$ process in the energy region $\sqrt{s} = 0.60$–0.97 GeV

M.N. Achasov, K.I. Beloborodov, A.V. Berdugin, A.G. Bogdanchikov, A.V. Bozhenok, A.D. Bukin, D.A. Bukin, T.V. Dimova, V.P. Druzhinin, V.B. Golubev, V.N. Ivanchenko, A.A. Korol *, S.V. Koshuba, E.V. Pakhtusova, A.A. Polunin, E.E. Pyata, A.A. Salnikov, S.I. Serednyakov, V.V. Shary, Yu.M. Shatunov, V.A. Sidorov, Z.K. Silagadze, A.N. Skrinsky, A.G. Skripkin, Yu.V. Usov, A.A. Valishev, A.V. Vasiljev

Budker Institute of Nuclear Physics, Novosibirsk 630090, Russia

Received 8 February 2003; received in revised form 24 February 2003; accepted 5 March 2003

Editor: L. Montanet

Abstract

Results of the study of the $e^+e^- \to \pi^0\gamma$ process with SND detector at VEPP-2M collider in the c.m.s. energy range $\sqrt{s} = 0.60$–0.97 GeV are presented. Using 36513 selected events, corresponding to a total integrated luminosity of 3.4 pb^{-1}, the $e^+e^- \to \pi^0\gamma$ cross section was measured. The energy dependence of the cross section was analyzed in the framework of the vector meson dominance model. The data are well described by a sum of $\phi, \omega, \rho \to \pi^0\gamma$ decay contributions with measured decay probabilities: $\mathrm{Br}(\omega \to \pi^0\gamma) = (9.34 \pm 0.15 \pm 0.31)\%$ and $\mathrm{Br}(\rho^0 \to \pi^0\gamma) = (5.15 \pm 1.16 \pm 0.73) \times 10^{-4}$. The ρ–ω relative interference phase is $\varphi_{\rho\omega} = (-10.2 \pm 6.5 \pm 2.5)$ degrees.

PACS: 13.40.Hq; 13.65.+i; 14.40.Cs

Keywords: Magnetic dipole transitions; Rho meson; Omega meson; Cross section

1. Introduction

The cross section of the $e^+e^- \to \pi^0\gamma$ process at c.m.s. energies $\sqrt{s} = 0.60$–0.97 GeV within the framework of the vector meson dominance model is determined by radiative decays of light vector mesons $\rho^0(770)$, $\omega(782)$, $\phi(1020)$. These decays, belonging to the class of magnetic dipole transitions, represent major interest as a probe of the quark structure of vector mesons, and for tests of low-energy models of strong interactions, such as a non-relativistic quark model, effective potential models, etc., [1–5]. Study of this process allows to improve accuracy of parameters of the $\rho^0, \omega \to \pi^0\gamma$ decays.

The only previous measurement of the decay $\rho^0 \to \pi^0\gamma$ was carried out by ND detector [6]: $\mathrm{Br}(\rho^0 \to \pi^0\gamma) = (7.9 \pm 2.0) \times 10^{-4}$. This result agrees with the PDG value for the isotopically complementary chan-

* Corresponding author.
E-mail address: a.a.korol@inp.nsk.su (A.A. Korol).

0370-2693
doi:10.1016/S0370-2693(03)00336-8

nel: $\mathrm{Br}(\rho^{\pm} \to \pi^{\pm}\gamma) = (4.5 \pm 0.5) \times 10^{-4}$ [7]. The $\omega \to \pi^0\gamma$ decay was studied in several experiments [6,8–12]. The current world average $\mathrm{Br}(\omega \to \pi^0\gamma)$ is equal to $(8.7 \pm 0.4)\%$ [7].

In this work we present the study of the $e^+e^- \to \pi^0\gamma$ process with SND detector at VEPP-2M collider.

2. Detector and experiment

The SND detector [13] consists of an electromagnetic calorimeter, tracking and muon systems. The main part of the detector is a three-layer spherical electromagnetic calorimeter consisting of 1600 NaI(Tl) crystals. The total thickness of the calorimeter for particles flying from the interaction point is $13.4X_0$, the total solid angle is $90\% \cdot 4\pi$. Energy resolution of the calorimeter for photons is $\sigma_E/E \approx 4.2\%/E\ (\mathrm{GeV})^{1/4}$, the angular resolution is $\sigma_{\varphi,\theta} \approx 0.82^\circ/\sqrt{E\ (\mathrm{GeV})} \oplus 0.63^\circ$.

The experiment was carried out at VEPP-2M collider [14]. The data were collected in March–July, 1998 [15] at 30 energy points in the range $\sqrt{s} = 0.60$–0.97 GeV. The total integrated luminosity of 3.4 pb^{-1} was used for the analysis. The beam energy determination was based on measurements of the magnetic field in the bending magnets and the beam revolution frequency in the collider. The error of the center of mass energy determination consists of two parts: relative accuracy of the energy setting for each energy point, which is equal to 0.1 MeV, and a 0.2 MeV general energy scale bias, common for all points within the experiment.

3. Data analysis

In this work the process $e^+e^- \to \pi^0\gamma$ was studied in the three-photon final state. The main sources of background are the QED processes $e^+e^- \to 3\gamma$ and $e^+e^- \to 2\gamma$ with extra photons of the machine background. Other possible sources are the process $e^+e^- \to \eta\gamma$ and cosmic background.

3.1. Events selection

For an event to be recorded, the SND first level trigger (FLT) required at least two clusters of hit crystals in the calorimeter and no signals in neither tracking nor muon systems. The FLT threshold on a calorimeter energy deposition changed with the beam energy, but was always below $0.4\sqrt{s}$.

The reconstructed events were first put through primary selection, which required at least 3 neutral and no charged particles, total energy deposition $E_{\mathrm{tot}} > 0.65\sqrt{s}$, total momentum measured by the calorimeter $P_{\mathrm{tot}} < 0.3\sqrt{s}$, polar angles of the two highest energy photons $36^\circ < \theta_{1,2} < 144^\circ$, the polar angle of the third photon (descending order in energy) $27^\circ < \theta_3 < 153^\circ$, and the energy deposition of this photon $E_{\gamma 3} > 0.1\sqrt{s}$. These conditions select three-photon events, while suppressing machine background and two photon annihilation events with additional background clusters in the calorimeter. As a result 52415 events were selected for further analysis.

In order to improve energy and angular resolutions for photons, the selected events were kinematically fitted under total energy and momentum conservation constraints. The fit results are the value of $\chi^2_{3\gamma}$ of the hypothesis and fitted kinematic parameters of the photons. The kinematic fit improves invariant mass resolution for photon pairs from π^0 decays from 11.2 to 8.6 MeV (Fig. 1).

The $\chi^2_{3\gamma}$ distribution is shown in Fig. 2. For additional suppression of the cosmic and machine backgrounds, we required $\chi^2_{3\gamma} < 20$. This cut also implicitly limits the maximum energy of initial state radiation (ISR) photons in the process under study (Fig. 3). In order to suppress the 2-photon annihilation background, each selected event was kinematically fitted to the $e^+e^- \to 2\gamma$ hypothesis, and restriction on calculated $\chi^2_{2\gamma}$ was applied: $\chi^2_{3\gamma} - \chi^2_{2\gamma} < 0$. The $\chi^2_{3\gamma} - \chi^2_{2\gamma}$ distribution is shown in Fig. 2.

The only significant backgrounds to the process under study remaining after described above cuts are the $e^+e^- \to \eta\gamma$ and QED 3γ annihilation. In the latter process all kinematically allowed combinations of the photon energies and angles are present, so this background cannot be completely eliminated by selection cuts and must be subtracted. To this end, all events, which passed primary selection and kinematic fit cuts, were divided into two classes: events with 108 MeV $\leqslant m_{\gamma\gamma} \leqslant$ 162 MeV were assigned to a class ***A***, the rest—to a class ***B***. Here $m_{\gamma\gamma}$ is an invariant mass of a photon pair after kinematic fitting (Fig. 1). The total number of the selected class ***A***

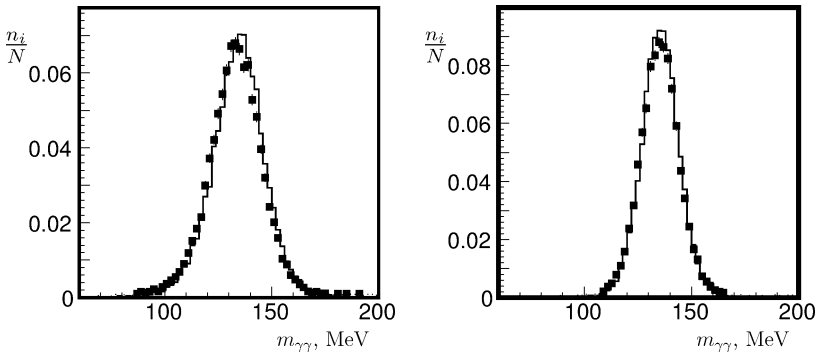

Fig. 1. Invariant mass distribution of photons pairs in the $e^+e^- \to \pi^0\gamma$ events before (left) and after (right) kinematic fitting. Solid line—MC simulation, points—data ($\sqrt{s} = 782$ MeV).

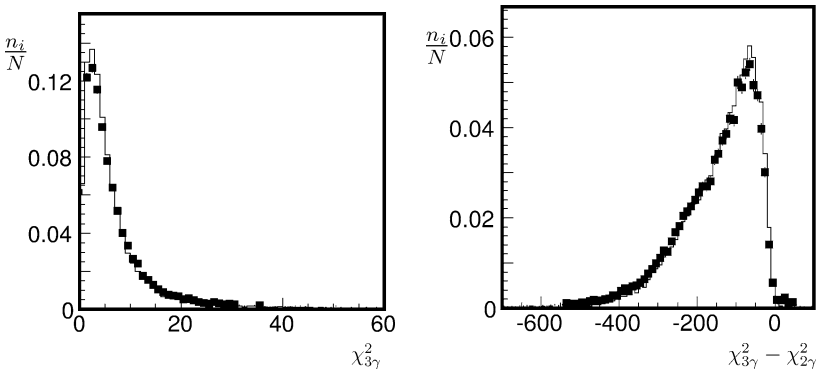

Fig. 2. The $\chi^2_{3\gamma}$ (left) and $\chi^2_{3\gamma} - \chi^2_{2\gamma}$ (right) distributions for the class ***A*** events. Solid line—MC simulation, points—data ($\sqrt{s} = 782$ MeV).

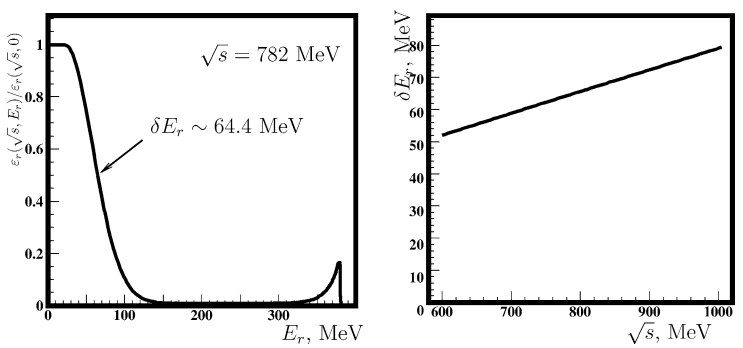

Fig. 3. Detection efficiency as a function of the ISR photon energy $\varepsilon_r(\sqrt{s}, E_r)$ for $\sqrt{s} = 782$ MeV (left), and effective ISR photon energy threshold δE_r (right) as a function of $\sqrt{s}$.

events is 36513. The fraction of the $e^+e^- \to \eta\gamma$ background in this class is less than 0.1%. For the class $\boldsymbol{B}$, this fraction is up to 5%. For calculation of the integrated luminosity a special sample of the $e^+e^- \to 2\gamma$ events (class $\boldsymbol{C}$) was selected using following criteria: no charged particles, at least two neutral particles, energy depositions for two most energetic photons $E_{p1,2} > 0.3\sqrt{s}$, their polar angles $36^\circ < \theta_{1,2} < 144^\circ$, azimuth acollinearity $\Delta\varphi_{12} < 10^\circ$, polar acollinearity $\Delta\theta_{12} < 25^\circ$, an event does not belong to classes $\boldsymbol{A}$ or $\boldsymbol{B}$. It is necessary to note significant contribution of the $e^+e^- \to \pi^0\gamma$ events to the class $\boldsymbol{C}$ (up to 10% at $\omega(782)$ resonance).

3.2. Cross section parameterization

The $e^+e^- \to \pi^0\gamma$ cross section in the framework of VDM can be parameterized as follows [16,17]:

$$\sigma_{\pi^0\gamma}(s) = \frac{(4\pi)^2\alpha \cdot q(s)^3}{3s^{3/2}} \times \left| \sum_{V=\rho,\omega,\phi} \frac{g_{\gamma V} \cdot g_{V\pi^0\gamma}}{D_V(s)} + A_{\text{non-res}} \right|^2, \quad (1)$$

$$D_V(s) = m_V^2 - s - i\sqrt{s}\,\Gamma_V(s), \quad (2)$$

$$q(s) = \frac{\sqrt{s}}{2}\left(1 - \frac{m_{\pi^0}^2}{s}\right). \quad (3)$$

Here $g_{\gamma V}$ and $g_{V\pi^0\gamma}$ are coupling constants, m_V is the V resonance mass, $\Gamma_V(s)$ is the energy-dependent width of the resonance, taking into account processes with branching ratios larger than 1%, $A_{\text{non-res}}$, represents possible non-resonant contribution. Using following formulas for the coupling constants:

$$|g_{\gamma V}| = \sqrt{\frac{m_V^5}{(4\pi)^2\alpha}\Gamma_V\sigma_V}, \quad (4)$$

$$|g_{V\pi^0\gamma}| = \sqrt{\frac{3\Gamma_V}{q(m_V^2)^3}\frac{\sigma_{V\pi^0\gamma}}{\sigma_V}}, \quad (5)$$

where σ_V and $\sigma_{V\pi^0\gamma}$ are the cross sections of the $e^+e^- \to V$ and $e^+e^- \to V \to \pi^0\gamma$ for $\sqrt{s} = m_V$, the Eq. (1) can be transformed to the form more suitable for data approximation:

$$\sigma_{\pi^0\gamma}(s) = \frac{q(s)^3}{s^{3/2}}\left|A_{\rho^0\pi^0\gamma}(s) + A_{\omega\pi^0\gamma}(s) + A_{\phi\pi^0\gamma}(s) + a_{\pi^0\gamma}\right|^2, \quad (6)$$

$$A_{V\pi^0\gamma}(s) = \frac{m_V\Gamma_V f_V(s)}{D_V(s)}\sqrt{\frac{m_V^3}{q(m_V^2)^3}\sigma_{V\pi^0\gamma}}, \quad (7)$$

where $a_{\pi^0\gamma}$ is a non-resonant contribution. We used two different models for the description of the interference phase between $\rho, \omega \to \pi^0\gamma$ decay amplitudes. For the model with energy-independent interference phases, $f_{\rho,\phi} = e^{i\varphi_{\rho,\phi}}$, $f_\omega \equiv 1$. In this case the φ_ρ is expected to be zero for pure ρ and ω isotopic states. Electromagnetic ρ–ω mixing gives rise to a non-zero φ_ρ value, which can be estimated from the $\text{Br}(\omega \to 2\pi)$: $\varphi_\rho \approx -13^\circ$. The second model is based on a mixed propagator approach [17,18]:

$$f_{\rho,\omega}(s) = \frac{r_{\rho,\omega}(s)}{|r_{\rho,\omega}(m_{\rho,\omega}^2)|}, \qquad f_\phi(s) = e^{i\varphi_\phi}, \quad (8)$$

$$r_\omega(s) = 1 + \varepsilon(s)\cdot\left(\frac{|g_{\gamma\rho^0}|}{|g_{\gamma\omega}|} + \frac{|g_{\rho^0\pi^0\gamma}|}{|g_{\omega\pi^0\gamma}|}\right), \quad (9)$$

$$r_\rho(s) = 1 - \varepsilon(s)\cdot\left(\frac{|g_{\gamma\omega}|}{|g_{\gamma\rho^0}|} + \frac{|g_{\omega\pi^0\gamma}|}{|g_{\rho^0\pi^0\gamma}|}\right), \quad (10)$$

$$\varepsilon(s) = \frac{\Pi_{\rho\omega}}{D_\omega(s) - D_\rho(s)}, \quad (11)$$

where $\Pi_{\rho\omega}$ is a ρ–ω mixing self-energy.

The detection efficiency for the $e^+e^- \to \pi^0\gamma$ process depends not only on $\sqrt{s}$, but also on energy of extra photons emitted by initial particles E_r. The detection efficiency $\varepsilon_r(\sqrt{s}, E_r)$ was determined by Monte Carlo simulation with the ISR taken into account. The energy and angular distributions of the ISR photons were generated according to Refs. [19,20]. The dependence of the detection efficiency on E_r, approximated by a smooth function, is shown in Fig. 3 for $\sqrt{s} = 782$ MeV. The noticeable peak in detection efficiency near ISR kinematic limit corresponds to the case when $\pi^0\gamma$ invariant mass is close to m_{π^0} and an ISR photon is emitted at large angle and detected. The effective threshold on the ISR photon energy $\delta E_r(s)$ is determined by χ^2 restriction. It can be defined as a width at half maximum of the $\varepsilon_r(\sqrt{s}, E_r)$. At $\sqrt{s} = 782$ MeV $\delta E_r \approx 64.4$ MeV. The δE_r dependence on $\sqrt{s}$ is shown in Fig. 3.

The visible cross section of the $e^+e^- \to \pi^0\gamma$ process was calculated as in [24]:

$$\sigma_{\pi^0\gamma,\mathrm{vis}}(s) = \int_0^{2E_{r,\max}/\sqrt{s}} \varepsilon_r\left(\sqrt{s}, \frac{x\sqrt{s}}{2}\right) F(x,s) \times \sigma_{\pi^0\gamma}\big((1-x)s\big)\,dx, \quad (12)$$

where $\sigma_{\pi^0\gamma}(s)$ is the process cross section (Eq. (6)), the function $F(x,s)$ is an electron "radiator" function [19]. For data presentation we used the traditional form:

$$\sigma_{\pi^0\gamma,\mathrm{vis}}(s) = \varepsilon\big(\sqrt{s}\big)\cdot\beta\big(\sqrt{s}\big)\cdot\sigma_{\pi^0\gamma}(s),$$

where $\varepsilon(\sqrt{s})$ and $\beta(\sqrt{s})$ are defined as:

$$\varepsilon\big(\sqrt{s}\big) \equiv \varepsilon_r(\sqrt{s},0), \quad (13)$$

$$\beta\big(\sqrt{s}\big) \equiv \frac{\int_0^{\frac{2E_{r,\max}}{\sqrt{s}}} \varepsilon_r(\sqrt{s}, \frac{x\sqrt{s}}{2}) F(x,s)\sigma_{\pi^0\gamma}((1-x)s)\,dx}{\varepsilon_r(\sqrt{s},0)\cdot\sigma_{\pi^0\gamma}(s)}. \quad (14)$$

For simulation of the background process $e^+e^- \to 3\gamma$ (QED) the lowest-order formulas from [21] were used. Visible cross section, calculated using Monte Carlo simulation, was corrected for higher order loop diagrams and soft photons emission [22] using δE_r as an upper limit of soft photons energy. The correction varied in the range of 0.915–0.925. We expect that the accuracy of the calculated $e^+e^- \to 3\gamma$ visible cross section is not worse than 2%.

For simulation of the process $e^+e^- \to 2\gamma$ (QED), used for luminosity determination, the formula from [23], taking into account additional photon emission, was used. The accuracy of the visible cross section determination is estimated to be 1%.

3.3. Data approximation

The FIT package [24] was used for data fitting. The fitting was done by means of the maximum likelihood method on all three data sets (classes ***A***, ***B***, and ***C***) simultaneously. Expected number of events in the ith energy point was calculated as:

$$N_i^{(j)} = IL_i\cdot\big(\sigma^{(j)}_{\pi^0\gamma,\mathrm{vis}}(E_i) + \sigma^{(j)}_{3\gamma,\mathrm{vis}}(E_i) + \sigma^{(j)}_{\eta\gamma,\mathrm{vis}}(E_i)\big), \quad j = A, B,$$

$$IL_i = \frac{N_i^{(C)}}{\sigma^{(C)}_{2\gamma,\mathrm{vis}}(E_i) + \sigma^{(C)}_{\pi^0\gamma}(E_i)}.$$

Visible hadronic cross sections were calculated according to Eq. (12) and corrected for the beam energy spread. Because the $e^+e^- \to \pi^0\gamma$ process gives noticeable contribution to the events of the luminosity process $e^+e^- \to 2\gamma$, the integrated luminosity (IL_i) was recalculated on every iteration step of the minimization. Our accuracy of the c.m.s. energy determination is worse than the accuracy of the ω-meson mass value. Therefore, we introduced possible energy scale bias ΔE as a free parameter. Other fit parameters were $\sigma_{\omega\pi^0\gamma}$, $\sigma_{\rho\pi^0\gamma}$, $a_{\pi^0\gamma}$, $k_{3\gamma}$, and φ_ρ or $\Pi_{\rho\omega}$ depending on description of the phase factor (Eqs. (1)–(8)) calculation. The $k_{3\gamma}$ parameter is a ratio of the measured and calculated $\sigma_{3\gamma}$ cross sections. Parameters of the $e^+e^- \to \phi \to \pi^0\gamma$ reaction were taken from [25]:

$$\sigma_{\phi\pi^0\gamma} = 5.12 \pm 0.39\ \mathrm{nb}, \quad (15)$$

$$\varphi_\phi = 158^\circ \pm 11^\circ. \quad (16)$$

For other cross section parameters the world average values [7] were used.

The data were approximated in the following four models:

(1) $\sigma_{\rho^0\pi^0\gamma} = 0$, $a_{\pi^0\gamma} = 0$;
(2) $\sigma_{\rho^0\pi^0\gamma}$ and φ_{ρ^0} are free parameters, $a_{\pi^0\gamma} = 0$;
(3) $\sigma_{\rho^0\pi^0\gamma}$ and $\Pi_{\rho\omega}$ are free parameters, $a_{\pi^0\gamma} = 0$;
(4) $\sigma_{\rho^0\pi^0\gamma}$ is a free parameter, $a_{\pi^0\gamma}$ is a free real parameter, $\Pi_{\rho\omega}$ is calculated from $\mathrm{Br}(\omega \to 2\pi)$.

Fitted energy scale bias $\Delta E = (-0.34 \pm 0.08)$ MeV for all models is consistent with our expectations. Found value of $k_{3\gamma}$ is $98.7 \pm 1.3\%$ with $\chi^2/N = 26/29$ shows good agreement between calculated and measured QED 3γ annihilation cross sections. For background subtraction we used the measured 3γ cross section. Other obtained parameters are listed in Table 1.

Large χ^2 value for the first model shows that the $e^+e^- \to \pi^0\gamma$ cross section cannot be described only by ω and ϕ decays contribution. The second model corresponds to an energy independent ρ–ω interference phase. Obtained value of this phase $(-10.2 \pm 6.5)^\circ$ is in agreement with expected for electromagnetic ρ–ω mixing $\varphi_\rho = (-12.8 \pm 1.1)^\circ$. Therefore,

Table 1
The fitted cross section parameters for different models. Only statistical errors are indicated

	$\sigma_{\omega\pi^0\gamma}$ (nb)	$\sigma_{\rho^0\pi^0\gamma}$ (nb)	$\varphi_{\rho\omega}$, degrees	$\Pi_{\rho\omega}$ (MeV^2)	Re $a_{\pi^0\gamma}$ (nb$^{1/2}$)	χ^2/N
1	176.6 ± 1.4	0			0	81/28
2	155.8 ± 2.7	0.58 ± 0.13	-10.2 ± 6.5		0	21.6/26
3	155.9 ± 2.7	0.56 ± 0.13	-9.9 ± 6.5[a]	-2819 ± 1841	0	21.9/26
4	156.8 ± 2.8	0.51 ± 0.13	-12.8 ± 1.1[a]	-3676 ± 303[b]	-0.13 ± 0.13	20.7/25

[a] Calculated using Eqs. (8)–(11).
[b] Derived from Br($\omega \to 2\pi$).

the last two fits were performed in the mixed propagator approach (Eq. (8)). The mixing self-energy $\Pi_{\rho\omega}$ was taken as a free parameter for the model 3 and calculated from the world average Br($\omega \to 2\pi$) for the model 4. The model 4 was used to estimate the contribution from the higher vector resonances ρ', ω', which was introduced as a pure real parameter $a_{\pi^0\gamma}$. The fitted $a_{\pi^0\gamma}$ value is compatible with zero. All the models 2–4 describe the experimental data equally well.

3.4. Systematic errors

Systematic error contributions for obtained cross section parameters are summarized in the Table 2.

The systematic error of luminosity determination originates mostly from inaccuracy of the $e^+e^- \to 2\gamma$ process cross section calculation (1%) and uncertainty of detection efficiency of the luminosity process, which was estimated using different angle and acollinearity selection cuts. The total error of the integrated luminosity determination was ~ 2–3%.

Primary selection efficiency depends on simple kinematic cuts and is independent of the c.m.s. energy. Thus, its systematic error emerging from simulation inaccuracy was studied by comparison of simulated and experimental event distributions at ω-resonance peak, where backgrounds are negligible. Systematic error of the primary selection efficiency does not exceed 1.5%.

The machine background changed with c.m.s. energy. In order to study its influence upon the detection efficiency we admixed recorded experimental background detector hits to simulated events. Comparison of the detection efficiencies obtained by simulation with and without machine background hits gives the estimate of the detection efficiency error from this source, not exceeding 0.5%.

Table 2
Contributions to the systematic errors of the cross section parameters

Source	$\sigma_{\omega\pi^0\gamma}$	$\sigma_{\rho^0\pi^0\gamma}$	φ
Integrated luminosity	2.0%	3.1%	0.8°
Three photons selection efficiency	1.5%	1.5%	0.4°
Final selection efficiency	1.6%	5.6%	2.2°
Additional clusters	0.3%	1%	0.2°
PDG table errors	0.1%	4%	0.4°
Total (no model error)	3.0%	7.8%	2.4°

The final class ***A*** selection criteria contain cuts in invariant masses and complex kinematic parameters $\chi^2_{3\gamma}$, $\chi^2_{2\gamma}$. Dependences of their efficiencies on c.m.s. energy and ISR photon energy in experiment and simulation may differ. In order to evaluate systematic error coming from this source, approximations were done with different cuts in these parameters.

Substantial systematic error contributions to the $\sigma_{\rho^0\pi^0\gamma}$ and φ come from inaccuracy of PDG data, mostly from the Γ_ω uncertainty.

4. Results

Our final results are based on the model 2 approximation. Differences in approximation results for the models 2–4 were considered as model error contributions to total systematic errors. As a result we present:

$$\sigma_{e^+e^-\to\omega\to\pi^0\gamma} = (155.8 \pm 2.7 \pm 4.8)\ \text{nb}, \quad (17)$$

$$\sigma_{e^+e^-\to\rho^0\to\pi^0\gamma} = (0.58 \pm 0.13 \pm 0.08)\ \text{nb}, \quad (18)$$

$$\varphi_{\rho\omega} = (-10.2 \pm 6.5 \pm 2.5)\ \text{degrees}. \quad (19)$$

Detailed point by point listing of the measured $e^+e^- \to \pi^0\gamma$ cross section is presented in Table 3. The systematic error of the experimental cross section is determined by systematic errors of integrated lumi-

Table 3
The $e^+e^- \to \pi^0\gamma$ cross section. δE is a c.m.s. energy spread, IL is an integrated luminosity, N is a number of events, $N_{\rm bg}$ is an estimated number of background events, $\varepsilon_{\pi^0\gamma}$ is a detection efficiency (Eq. (13)) of the process $e^+e^- \to \pi^0\gamma$, $\beta_{\pi^0\gamma}$ is a factor taking into account radiative correction (Eq. (14)) and beam energy spread. The c.m.s. energy ($\sqrt{s}$) is corrected according to fitted ΔE. Its error is 0.08 MeV. The first error of the cross section $\sigma_{\pi^0\gamma}$ is statistical, the second one is systematic

$\sqrt{s}$ (MeV)	δE (MeV)	IL ($\rm nb^{-1}$)	N	$N_{\rm bg}$	$\varepsilon_{\pi^0\gamma}$	$\beta_{\pi^0\gamma}$	$\sigma_{\pi^0\gamma}$ (nb)
599.52	0.14	39.90 ± 0.30	60	46.0	0.315	0.908	$1.23 \pm 0.77 \pm 0.19$
629.51	0.15	46.09 ± 0.33	62	44.8	0.316	0.904	$1.31 \pm 0.68 \pm 0.43$
659.52	0.16	40.02 ± 0.33	37	32.0	0.313	0.899	$0.45 \pm 0.63 \pm 0.17$
689.56	0.19	48.31 ± 0.38	48	33.0	0.316	0.893	$1.10 \pm 0.59 \pm 0.30$
719.51	0.18	58.43 ± 0.43	69	36.0	0.323	0.886	$1.97 \pm 0.56 \pm 0.18$
749.50	0.20	50.90 ± 0.42	84	26.8	0.317	0.866	$4.09 \pm 0.73 \pm 0.28$
759.50	0.20	41.88 ± 0.39	107	20.7	0.316	0.846	$7.71 \pm 1.02 \pm 0.42$
763.50	0.21	38.80 ± 0.38	124	18.7	0.317	0.834	$10.27 \pm 1.19 \pm 0.47$
769.50	0.21	43.60 ± 0.40	234	20.3	0.319	0.812	$18.95 \pm 1.45 \pm 1.08$
773.50	0.21	62.77 ± 0.48	531	28.7	0.319	0.794	$31.62 \pm 1.51 \pm 1.45$
777.50	0.21	76.73 ± 0.53	1544	35.0	0.319	0.776	$79.60 \pm 2.13 \pm 2.15$
778.71	0.22	6.88 ± 0.16	162	3.2	0.319	0.772	$93.89 \pm 8.13 \pm 3.82$
779.48	0.24	43.39 ± 0.39	1282	20.0	0.319	0.770	$118.49 \pm 3.46 \pm 2.94$
780.59	0.23	132.36 ± 0.68	4989	61.4	0.319	0.772	$151.36 \pm 2.20 \pm 4.40$
781.63	0.24	351.62 ± 1.10	15259	164.1	0.319	0.779	$172.82 \pm 1.43 \pm 5.15$
782.52	0.21	81.11 ± 0.53	3523	37.8	0.319	0.793	$169.83 \pm 2.94 \pm 4.76$
783.51	0.21	74.90 ± 0.51	3150	34.7	0.319	0.816	$159.53 \pm 2.93 \pm 5.46$
785.51	0.22	73.73 ± 0.51	2391	33.3	0.320	0.883	$113.15 \pm 2.39 \pm 3.18$
789.50	0.22	56.91 ± 0.46	930	24.6	0.320	1.044	$47.61 \pm 1.66 \pm 1.43$
793.49	0.23	53.03 ± 0.45	456	22.4	0.320	1.201	$21.26 \pm 1.10 \pm 0.80$
799.49	0.23	51.86 ± 0.45	285	21.3	0.320	1.411	$11.27 \pm 0.77 \pm 0.31$
809.49	0.25	65.73 ± 0.52	189	25.8	0.318	1.660	$4.70 \pm 0.43 \pm 0.13$
819.49	0.24	115.74 ± 0.70	233	43.7	0.318	1.775	$2.90 \pm 0.25 \pm 0.19$
839.47	0.25	144.83 ± 0.80	179	52.6	0.320	1.711	$1.59 \pm 0.18 \pm 0.07$
879.45	0.27	170.26 ± 0.91	100	50.4	0.318	1.269	$0.72 \pm 0.16 \pm 0.17$
919.43	0.32	327.70 ± 1.32	137	77.7	0.319	1.048	$0.54 \pm 0.12 \pm 0.04$
939.45	0.30	291.22 ± 1.28	99	63.0	0.318	1.007	$0.39 \pm 0.12 \pm 0.09$
949.45	0.29	259.10 ± 1.22	86	53.9	0.317	0.993	$0.39 \pm 0.13 \pm 0.06$
957.45	0.29	241.63 ± 1.18	79	48.8	0.317	0.984	$0.40 \pm 0.13 \pm 0.06$
969.46	0.30	245.65 ± 1.21	84	47.6	0.319	0.969	$0.48 \pm 0.13 \pm 0.10$

nosity, detection efficiency, radiative correction, and background subtraction. It is worth mentioning that systematic errors for different c.m.s. energy points are highly correlated. The measured cross section and data from [6,25] are also plotted in Fig. 4.

Decay parameters expressed in terms of probabilities and partial widths are:

$$\mathrm{Br}\big(\omega \to \pi^0\gamma\big) \cdot \mathrm{Br}\big(\omega \to e^+e^-\big) = (6.50 \pm 0.11 \pm 0.20) \times 10^{-6}, \quad (20)$$

$$\mathrm{Br}\big(\rho \to \pi^0\gamma\big) \cdot \mathrm{Br}\big(\rho \to e^+e^-\big) = (2.34 \pm 0.53 \pm 0.33) \times 10^{-8}, \quad (21)$$

$$\mathrm{Br}\big(\omega \to \pi^0\gamma\big) = (9.34 \pm 0.15 \pm 0.31)\%, \quad (22)$$

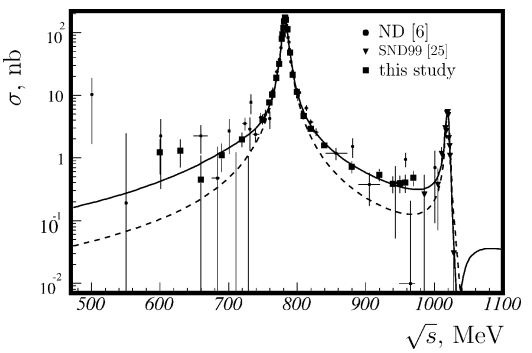

Fig. 4. $e^+e^- \to \pi^0\gamma$ cross section. Solid line depicts the cross section in the model 2, dashed line—in the model 1. The ND data are grouped by energies and shifted according to current world average value of the ω-meson mass.

$$\mathrm{Br}\left(\rho^0 \to \pi^0\gamma\right) = (5.15 \pm 1.16 \pm 0.73) \times 10^{-4}, \quad (23)$$

$$\Gamma_{\omega\to\pi^0\gamma} = (788 \pm 12 \pm 27)\ \mathrm{keV}, \quad (24)$$

$$\Gamma_{\rho^0\to\pi^0\gamma} = (77 \pm 17 \pm 11)\ \mathrm{keV}. \quad (25)$$

Obtained results statistically agree with previous measurements. The partial width $\Gamma_{\rho^0\to\pi^0\gamma}$ is in a good agreement with the world average $\Gamma_{\rho^\pm\to\pi^\pm\gamma}$. Phenomenological estimates using various models [1–5] do not contradict our result.

The ratio of the partial widths of the ω, $\rho \to \pi^0\gamma$ decays required by strict $SU(3)$ symmetry [2] is equal to 9.47, which is in agreement with our measurement:

$$\frac{\Gamma_{\omega\to\pi^0\gamma}}{\Gamma_{\rho^0\to\pi^0\gamma}} = 10.3 \pm 2.5 \pm 1.4. \quad (26)$$

5. Conclusions

The most accurate measurement of the $e^+e^- \to \pi^0\gamma$ cross section is performed in the c.m.s. energy region of 0.60–0.97 GeV at VEPP-2M collider with the SND detector. At present experimental accuracy level this cross section is well described by vector meson dominance model, taking into account $\phi, \omega, \rho \to \pi^0\gamma$ transitions. In this model the cross sections of the processes $e^+e^- \to \omega \to \pi^0\gamma$ and $e^+e^- \to \rho^0 \to \pi^0\gamma$ at corresponding meson masses are measured. Partial widths, their ratios, and decay probabilities of corresponding decays were evaluated. Results are presented in Eqs. (17)–(26) and in Table 3.

The measured values of the $\omega, \rho^0 \to \pi^0\gamma$ decay parameters are consistent with earlier experimental results. The partial width of the $\rho^0 \to \pi^0\gamma$ decay is in a good agreement with that of $\rho^\pm \to \pi^\pm\gamma$ decays. These values also do not contradict various phenomenological estimations. Obtained value of the ρ–ω interference phase could be well explained by electromagnetic ρ–ω mixing. Our results have higher accuracy than the world averages for the $\rho^0 \to \pi^0\gamma$ and $\omega \to \pi^0\gamma$ decay branching ratios.

Acknowledgements

This work was partially supported with RFBR grants 00-15-96802, 01-02-16934-a, and grant No. 781999 of Russian Academy of Science for young scientists.

References

[1] D.A. Geffen, W. Wilson, Phys. Rev. Lett. 44 (1980) 370.
[2] P.J. O'Donnell, Rev. Mod. Phys. 53 (1981) 673.
[3] P. Singer, G.A. Miller, Phys. Rev. D 33 (1986) 141.
[4] N. Barik, P.C. Dash, Phys. Rev. D 49 (1994) 299.
[5] S.-L. Zhu, et al., Phys. Lett. B 420 (1998) 8.
[6] S.I. Dolinsky, et al., Phys. Rep. 202 (1991) 99.
[7] K. Hagiwara, et al., Phys. Rev. D 66 (2002) 010001.
[8] F. Jacquet, et al., Nuovo Cimento 63A (1969) 743.
[9] A.B. Baldin, et al., Yad. Fiz. 13 (1971) 758.
[10] D. Benaksas, et al., Phys. Lett. B 42 (1972) 511.
[11] J. Keyne, et al., Phys. Rev. D 14 (1976) 28.
[12] V.M. Aulchenko, et al., J. Exp. Theor. Phys. 90 (2000) 927, Zh. Eksp. Teor. Fiz. 90 (2000) 1067.
[13] M.N. Achasov, et al., Nucl. Instrum. Methods A 449 (2000) 125.
[14] I.A. Koop, et al., Published in: Physics and detectors for DAPHNE, Frascati, 1999, pp. 393–404.
[15] M.N. Achasov, et al., Preprint Budker INP 98-65, Novosibirsk, 1998.
[16] N.N. Achasov, et al., Sov. J. Nucl. Phys. 54 (1991) 664, Yad. Fiz. 54 (1991) 1027;
N.N. Achasov, et al., Int. J. Mod. Phys. A 7 (1992) 3187.
[17] H.B. O'Connell, et al., Prog. Part. Nucl. Phys. 39 (1997) 201.
[18] N.N. Achasov, et al., Sov. J. Nucl. Phys. 55 (1992) 449, Yad. Fiz. 55 (1992) 809;
N.N. Achasov, et al., Int. J. Mod. Phys. A 7 (1992) 4825.
[19] E.A. Kuraev, V.S. Fadin, Sov. J. Nucl. Phys. 41 (1985) 466, Yad. Fiz. 41 (1985) 733.
[20] G. Bonneau, F. Martin, Nucl. Phys. B 27 (1971) 381.
[21] A.B. Arbuzov, et al., JHEP 10 (1997) 001.
[22] E.A. Kuraev, Z.K. Silagadze, Phys. Atom. Nucl. 58 (1995) 1741, Yad. Fiz. 58 (1995) 1843.
[23] V.N. Baier, et al., Phys. Rep. 78 (1981) 293.
[24] A.V. Bozhenok, et al., Preprint Budker INP 99-103, Novosibirsk, 1999 (in Russian).
[25] M.N. Achasov, et al., Eur. Phys. J. C 12 (2000) 25.